Removal of phenol content of an industrial wastewater via a heterogeneous photodegradation process using supported FeO onto nanoparticles of Iranian clinoptilolite

Zarifeh-Alsadat Mirian[a], Alireza Nezamzadeh-Ejhieh[a,b,]*

[a]*Department of Chemistry, Shahreza Branch, Islamic Azad University, P.O. Box 311-86145, Shahreza, Isfahan, Iran,*
Tel. +98 31 53292515; Fax: +98 31 53291018; emails: z-mirian@hotmail.com (Z.-A. Mirian), arnezamzadeh@iaush.ac.ir
(A. Nezamzadeh-Ejhieh)
[b]*Razi Chemistry Research Center (RCRC), Shahreza Branch, Islamic Azad University, Isfahan, Iran, Tel. +98 31 53292500*

ABSTRACT

FeO was supported onto clinoptilolite nanoparticles and used in photodegradation of phenol in a wastewater sample under Hg lamp irradiation. Raw and modified samples were characterized by XRD, FTIR, DRS, TEM, and SEM. The effects of catalyst dosage, dilution extent of the used wastewater, initial pH, and doses of hydrogen peroxide and potassium bromate were studied on the degradation activity of the catalyst. The optimal operation parameters were found as: 38-mg L^{-1} phenol (five times of diluted solution), pH 6.7, and 0.3-g L^{-1} catalyst mass.

Keywords: Wastewater; Phenol; Heterogeneous catalysis; FeO; Nanoparticles; Clinoptilolite

1. Introduction

One of the most important topics of research area is the development of efficient methods to control or reduce environmental pollution, particularly removal of hazardous organic compounds from water resources [1,2]. Phenols are one of the most interested pollutants because of their toxicity, so the phenol content of drinking water should not exceed 2 μg L^{-1} [3]. Phenolic compounds can enter into the surface water from different industrial effluents such as disinfectant, the coal tar, plastic, gasoline, rubber proofing, pharmaceutical and steel industries, and domestic wastewaters, agricultural run-off, and chemical spills. Phenolic compounds also cause unpleasant taste and odor in drinking water [4].

Biodegradation of phenolic compounds is often inconvenient for the removal of phenols from wastewater because its toxicity may cause phototoxic effects on the active micro-organisms. In this point of view, increasing attention has been paid on complete degradation of organic pollutants to harmless products such as CO_2 and H_2O by the advanced oxidation processes (AOPs) [5,6]. In the recent two decades, AOP methods have been used as an useful technology in the treatment of wastewater samples to destroy/decrease their organic pollutants. In the AOP processes, sufficient quantities of highly reactive and non-selective hydroxyl radicals can be produced that have the ability to oxidize most of the toxic and hazardous organic species present in industrial effluents [7].

Among the various AOP methods, the semiconductor-mediated heterogeneous photocatalysis is an interesting and promising technique for environmental cleaning and remediation due to its potential to destroy a wide range of organic and inorganic pollutants at ambient temperatures and pressures. With an appropriate light irradiation, the proposed photocatalyst generates electron/hole pairs with free electrons produced in the empty conduction band. The produced electron/hole pairs can initiate a series of chemical reactions that eventually mineralize organic pollutants [8,9]. The use of semiconductors with nanodimensions in photocatalysis has generated great interest due to their unique physicochemical properties caused by their nanosized dimensions and large surface/volume ratio [10,11].

Iron oxides are natural minerals and geocatalysts widely existing in the earths' crust and also suspended in aqueous streams, aerosol, clouds, and fogs fine particles. The photodegradation of different organic pollutants on the surface of iron oxides is very feasible and useful for the removal of organic pollutants from contaminated water [12]. A Fe^{3+}–TiO_2-zeolite has been used for the photodegradation of methyl orange, which showed that the iron ions have an important role in the photocatalytic activity of the composite, so it can penetrate in the TiO_2 lattice and increase the TiO_2 absorbency [13]. In this research, for enhancement of the photocatalytic activity, iron(II) oxide was supported onto the nanoparticles of clinoptilolite zeolite. The supported nano-TiO_2 particles onto a polymeric matrix have been used in the photodegradation of phenol and its derivates [14] and the optimal values were obtained as: 1 g-L^{-1} catalyst at irradiation time of 10 h for a 10 mg-L^{-1} phenol solution. Comparison of these results with the present work (0.3 g-L^{-1} catalyst, irradiation time of 90 min, and phenol concentration of 96 mg L^{-1}) and also the use of real wastewater sample confirms the superiority of the proposed catalyst used in this work. In another study, $Fe(OH)^{2+}$–TiO_2 catalyst has been used for the degradation of phenol [15]. However, in the above-mentioned works, the synthesis of catalysts seeking high time and cost while using low-cost catalysts and rapid methods is important in the industrial applications.

In the present work, nanoparticles of natural clinoptilolite zeolite as an eco-friendly material was used as a suitable support for FeO. The obtained photocatalyst showed good activity for the degradation of phenol in a wastewater sample. The optimum values of experimental factors such as: pH, dilution extent of the wastewater sample, and dose of the catalyst were determined to reach the best photodegradation efficiency.

2. Experimental

2.1. Reagents

Ferro ammonium sulfate, hydrogen peroxide, potassium bromate, and other analytical grade chemicals are obtained from Merck. Natural clinoptilolite (CP) tuffs (belonging to the Semnan region in the northeast of Iran) are prepared from Afrand Touska Company (Isfahan-Iran). The pH of the solutions was appropriately adjusted with sodium hydroxide or hydrochloric acid solution. Distilled water was used throughout the experiments. The phenol wastewater sample was obtained from Isfahan Coal Tar refinery and its characteristics are summarized in Table 1.

2.2. Preparation of the zeolite

Natural clinoptilolite tuffs were mechanically pretreated by crushing in an agate mortar and sieving in analytical sieves. The obtained micronized powder was converted to nanoparticles using a planetary ball mill (PM100; Retsch Corporation). In order to remove any water soluble and magnetic impurities, the obtained nanoparticles were heated at 70°C in distilled water for 24 h in a magnetic stirrer. In order to reach a fixed water content, after centrifuging and drying, the pretreated powder was stored in a desiccator over saturated sodium chloride solution for two weeks.

2.3. Preparation of FeO-clinoptilolite

To prepare the FeO/nanoclinoptilolite powder (FeO–NCP), first the Fe(II)-exchanged clinoptilolite (Fe–NCP) was obtained by adding 10 g of nanoclinoptilolite powder (NCP) into a polyethylene bottle containing 25-mL 0.1 mol L^{-1} Fe^{2+} aqueous solution and the suspension was shaken for 24 h at room temperature. To complete the ion exchange process, this process was repeated again. At the end of the process, the obtained Fe–NCP particles were filtered off, washed with water, air dried during day, and finally it was calcined in an oven at 250°C for 10 h to obtain the FeO–NCP catalyst. A similar method was applied for 0.05, 0.2, and 0.3 M Fe(II) solutions.

Table 1
Characteristics of original wastewater sample

Parameter	Average value (mg L^{-1})
Phenol	190
TSS	172
TOC	3,500
COD	2050

2.4. Characterization methods

FT-IR spectra of the samples on KBr pellets were recorded with a Nicolet single beam FT-IR (Impact 400D) spectrometer in the range of 400–4,000 cm^{-1} at room temperature. The X-ray diffraction (XRD) patterns of samples were recorded using a Bruker diffractometer (D8 advance) with a Ni-filtered copper radiation (Kα = 1.5406 Å). The surface morphology of samples was studied using a Philips XL30 scanning electron microscope (SEM). The amount of Fe was measured by an atomic absorption spectrometer, Perkin Elmer AAnalyst 300 (Air-C$_2$H$_2$, λ = 352.5 nm). The diffuse reflectance spectroscopic (DRS) studies were carried out using Shimadzu UV 3600 equipped with an integrating sphere using BaSO$_4$ as the reference material. The absorption spectra were registered on a double-beam UV–vis spectrophotometer (Carry 100 Scan) in quartz cells of 1-cm optical path length in the wavelength range of 190–900 nm. The TEM images of samples were recorded using transmission electron microscope S-3500N with absorbed electron detector S-6542 (Hitachi Science System Ltd). The measurements of total organic carbon (TOC) were performed by TOC analyzer (Shimadzu TOC-VCSN).

2.5. Photodegradation experiments

In the preliminary experiments, the role of surface adsorption for the removal of pollutant was measured at dark condition. For this goal, an appropriate amount of the photocatalyst (for example, 0.3 g L^{-1} as the optimum value) was added to a 20-mL fivefold diluted wastewater sample. The suspension was shaken and at regular time intervals, the aliquot of the suspension was centrifuged. The comparison of absorbance of the cleaned solution at its λ_{max} = 270 nm with that of blank waste solution (without contacting with the catalyst) confirmed about 4% of phenol can be removed due to surface adsorption after 30 min and thereafter remained unchanged. Hence, before photodegradation experiments, suspensions were shaken for 30 min in dark to reach adsorption/desorption equilibrium (and hence, elimination of the role of surface adsorption on the removal of phenol). Also, direct photolysis of the sample (without the catalyst) confirmed maximum 5.5% removal of phenol after 120 min.

The experimental setup for the photodegradation of 20-mL wastewater solution containing 0.3-g L^{-1} photocatalyst (or other values for unoptimized conditions) was constructed in a cylindrical Pyrex glass cell (5 cm inside diameter and 10 cm height) as a reactor. The suspensions were irradiated under atmospheric condition with a medium pressure UV lamp (75 W, Philips) located 10-cm above the reactor. During the irradiation, the suspension was sampled out at regular time intervals and centrifuged to remove any suspended solid catalyst particles. Then absorption spectrum of the clear solution was recorded and the degradation extent was calculated in terms of the change in the absorbance at the λ_{max} = 270 nm. The degradation extent was calculated by the following equation:

$$\text{Degradation } \% = (A_0 - A_t/A_0) \times 100 \tag{1}$$

where A_0 and A_t are the blank and sample absorbances. A_0 and A_t relate to the initial (C_0) and final (C) concentrations according to the Beer–Lambert law, respectively.

In each case (especially in the study of pH, bromate, and hydrogen peroxide), blank solutions at similar condition with their corresponding suspensions irradiated and the reordered absorbencies of the sample and blank solutions were used for the calculation of degradation extent of phenol. Hence, the effect of surface adsorption, direct photolysis, and the effects of bromate and hydrogen peroxide (in the absence of the catalyst) eliminated in the reported degradation extents, and net photodegradation extents were reported.

3. Results and discussion

3.1. Characterization

3.1.1. FT-IR investigation

FT-IR lattice vibration spectra were used to investigate the influence of Fe(II) and FeO on the zeolite framework. The representative spectra of NCP, Fe-nano clinoptilolite (Fe–NCP), and FeO-nanoclinoptilolite (FeO–NCP) are shown in Fig. 1. According to the spectrum (a) in Fig. 1, the peaks located at 1,645, 1,069, 792, 606, and 470 cm^{-1} are in good agreement with the infrared spectral data reported for clinoptilolite in the literature [16]. Infrared spectroscopy reflects the changes of the framework configurations of the zeolite host after the incorporation of the guests. Changes in the characteristic bands take place between the host NCP and the host–guest Fe–NCP and FeO–NCP samples, so the deformation modes of water in the range of 1,625–1,640 cm^{-1} and the OH stretching band at 3,470 cm^{-1} are clearly seen in the treated Fe–NCP and FeO–NCP samples. These observations are in accordance with the literature [17]. For Fe–NCP, the characteristic bands are seen at 469 (470) cm^{-1}, 606
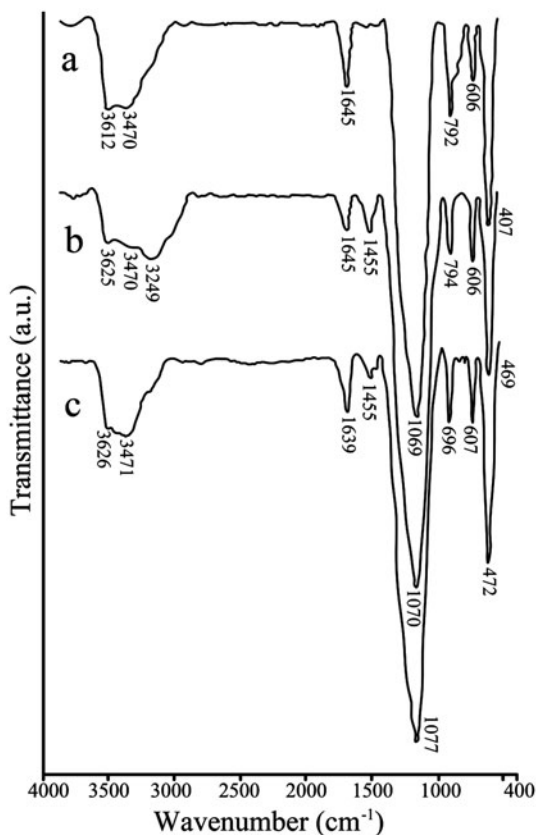
Fig. 1. FT-IR spectra of (a) NCP, (b) Fe–NCP, and (c) FeO–NCP.

(606) cm^{-1} (T–O bending), 794 (792) cm^{-1} (symmetrical stretching), and 1,070 (1,069) cm^{-1} (asymmetrical stretching) that show small shifts for some bands with respect to the bands of the NCP host (wavenumbers in the parenthesis) (Fig. 1(a) and (b)).

Based on the FT-IR results, the peak located at 1,069 cm^{-1} is attributed to asymmetric O–T–O (T=Al or Si) stretching vibration in clinoptilolite which is present in all zeolitic structures and is sensitive to the content of the framework Si/Al ratio. As shown, negligible shifts were observed for this peak in the ion-exchanged and calcined samples. This confirms that the original structure of the zeolite remains unchanged during these processes and no Al or Si removal was happened. For treated samples, the changes for OH vibration modes are significant. The located band at 3,612 cm^{-1} for clinoptilolite corresponds to the bridging OH groups in Al–OH–Si and is attributed to the location of hydrogen atoms on different oxygen atoms of zeolite framework [18,19]. This band was shifted to higher energies in the treated samples indicating the difficulty of the vibration. The

active ion exchange or complexation sites of zeolites are Si–OH–Al, Si–OH and Al–OH functional groups, which will be negatively charged by removing one H-atom. Intermolecular hydrogen bonding causes the appearance of bands at 3,550–3,200 cm^{-1} for "monomeric" and "polymeric" structures [20]. For the used clinoptilolite sample, the corresponding vibrations were observed at 3,470 and 3,612 cm^{-1}, and also a shoulder at 3,238 cm^{-1} which are in good agreement with the literature [21]. By entering Fe(II) cations into the clinoptilolite structure, the mentioned shoulder is converted to a strong peak at 3,249 cm^{-1} corresponding to the polymeric hydrogen bonds while the peak located at 3,470 cm^{-1} corresponds to monomeric hydrogen bonds. This observation is desirable due to the formation of various oxo- and hydroxo-species of iron(II) cations which can form hydrogen bonds extensively [18]. Especially, the formation of Al–O–Fe–(OH) significantly increases chemisorbed and physically sorbed water molecules. The amount of the adsorbed water molecules depends on the type of oxide and, to a greater extent, on the surface area. Hence, some changes take place in the position and intensity of these peaks during the calcination process. The observed shifts towards lower energies indicate an increase in the hydrogen bonding for Fe–NCP [18–22].

3.1.2. XRD patterns

The XRD patterns of raw NCP, Fe–NCP, and FeO–NCP samples are shown in Fig. 2. The parent raw nanoparticles showed a pattern similar to the crystalline structure data of clinoptilolite according to JCPDS No. 39-1383 (lines in the XRD pattern) [23]. This confirms that the used tuffs include the clinoptilolite as a major phase (together with 3.9% quartz and 8.9% cristobalite as impurities). The FeO peaks are located in 2θ values equal to 34.5°, 41.0°, and 59.2° and the peaks of Al–Fe–SiO$_4$–O are located in 2θ values equal to 12°, 26°, 27°, 30°, 33°, and 36.1° [24]. The weak XRD lines of FeO in the pattern (c) are because of low-FeO loading by the zeolite. As obvious from the XRD results, the zeolite structure remained unchanged after the incorporation of Fe^{2+} and FeO, but the intensity of the peaks in the host–guest samples was decreased with respect to the raw NCP sample. These observations are in good agreement with the literature [25].

By analyzing the β, excess of width line of the diffraction peak in radians and θ, the Bragg angle in degrees, the average size of the raw and treated NCP particles can be calculated using the Scherer equation [26]:
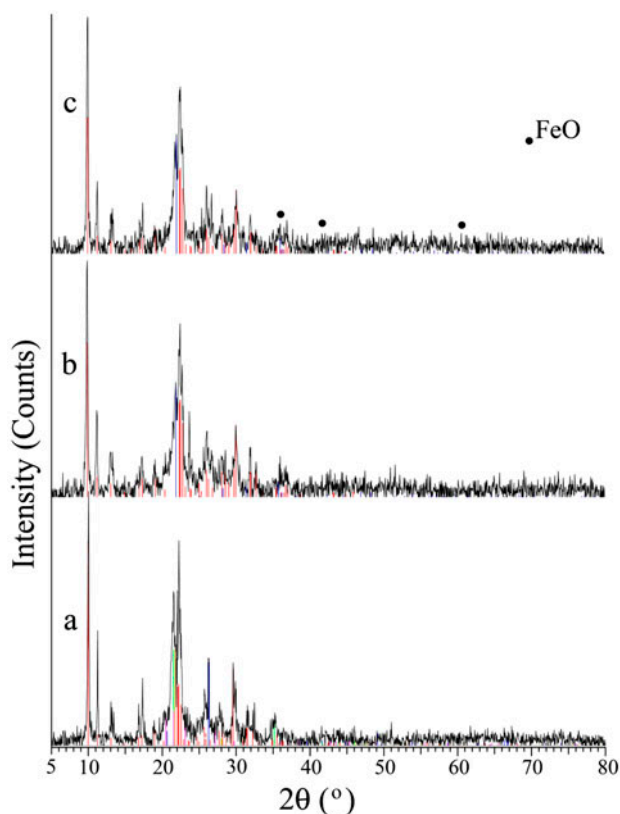
Fig. 2. X-ray diffraction patterns of (a) NCP, (b) Fe–NCP, and (c) FeO–NCP.

$$d = 0.9\lambda/\beta \cos \theta \qquad (2)$$

where d is the average diameter of the crystal and λ is the wavelength of X-ray photons. The average sizes of the NCP, Fe–NCP, and FeO–NCP particles were estimated about 22–30, 32–40, and 36–50 nm, respectively.

3.1.3. SEM and TEM studies

The surface morphology of the NCP (a), Fe–NCP (b), and FeO–NCP samples (c and d) was studied by SEM and the corresponding pictures are presented in Fig. 3. The crystallites of the unloaded zeolite have very well-defined layer-like crystals. The images of the loaded samples also show that the zeolite crystallites are not affected by the Fe^{2+} and FeO loading. In all images, although there are some larger particles, the major one has nanodimensions. As shown, the loading of FeO particles closes the pores of the parent clinoptilolite nanoparticles. The average particle sizes of NCP, Fe–NCP, and FeO–NCP were estimated about 25, 35, and 85.01 nm, respectively. Entering the Fe^{2+} and FeO into the zeolite structure led to an increase in

the particle sizes of Fe–NCP and FeO–NCP samples. Higher increase in the particle size of FeO–NCP in turn confirms the iron oxidation in the calcined form.

To have more information about the particle size of the prepared samples, the TEM images of nanoparticles of clinoptilolite and FeO–NCP were also recorded and the corresponding images are, respectively, shown in Fig. 3(e) and (f). As shown, major particles of clinoptilolite and FeO–NCP samples have sizes less than 100 nm. This confirms that the dimensions of NCP particles remained nearly unchanged during ion exchange and calcination processes. This also confirms that nanoparticles of FeO were formed inside and on the surface of NCP particles during calcination process.

3.1.4. UV–vis diffuse reflectance spectroscopy

The DRS results of the NCP, Fe–NCP, and FeO–NCP samples are shown in Fig. 4. For the raw NCP particles, spectral maxima appeared at 255 nm in the UV region, while in the Fe–NCP spectrum, a red shift towards 290 nm and two maximum observed at 320 and 490 nm which can be related to Fe bonded to the oxygen atoms of zeolite framework. These observations confirm the incorporation of Fe cations into the zeolite structure during the ion exchange process. DRS spectrum of FeO–NCP shows an increase in the absorbance intensity of the obtained composite. However, DRS results are in coherent with FT-IR, XRD, and SEM results confirming the formation of Fe–NCP catalyst. In addition to the instrumental characterization results, the change of dark white color of the Fe–NCP sample to dark red color of FeO–NCP after calcination process can be considered as a primary evidence for the change of Fe(II) to FeO.

3.2. Catalytic activity of FeO–NCP sample

3.2.1. Effect of FeO loaded on the photodegradation efficiency

As mentioned above, different FeO–NCP catalysts were prepared and their iron contents were determined using atomic absorption spectroscopy. The obtained results are summarized in Table 2. As shown, the FeO contents of 1.6, 3.2, 3.7, and 4.1% were, respectively, obtained for the catalysts prepared in 0.05, 0.1, 0.2, and 0.3 M of Fe^{2+} solutions. To study the influence of loaded FeO onto NCP on the degradation process, the photocatalytic activities of the prepared catalyst were studied at the same experimental conditions (0.1 g L^{-1} of the catalyst). Based on the results, $\ln(C_0/C)$ was plotted vs. irradiation time and
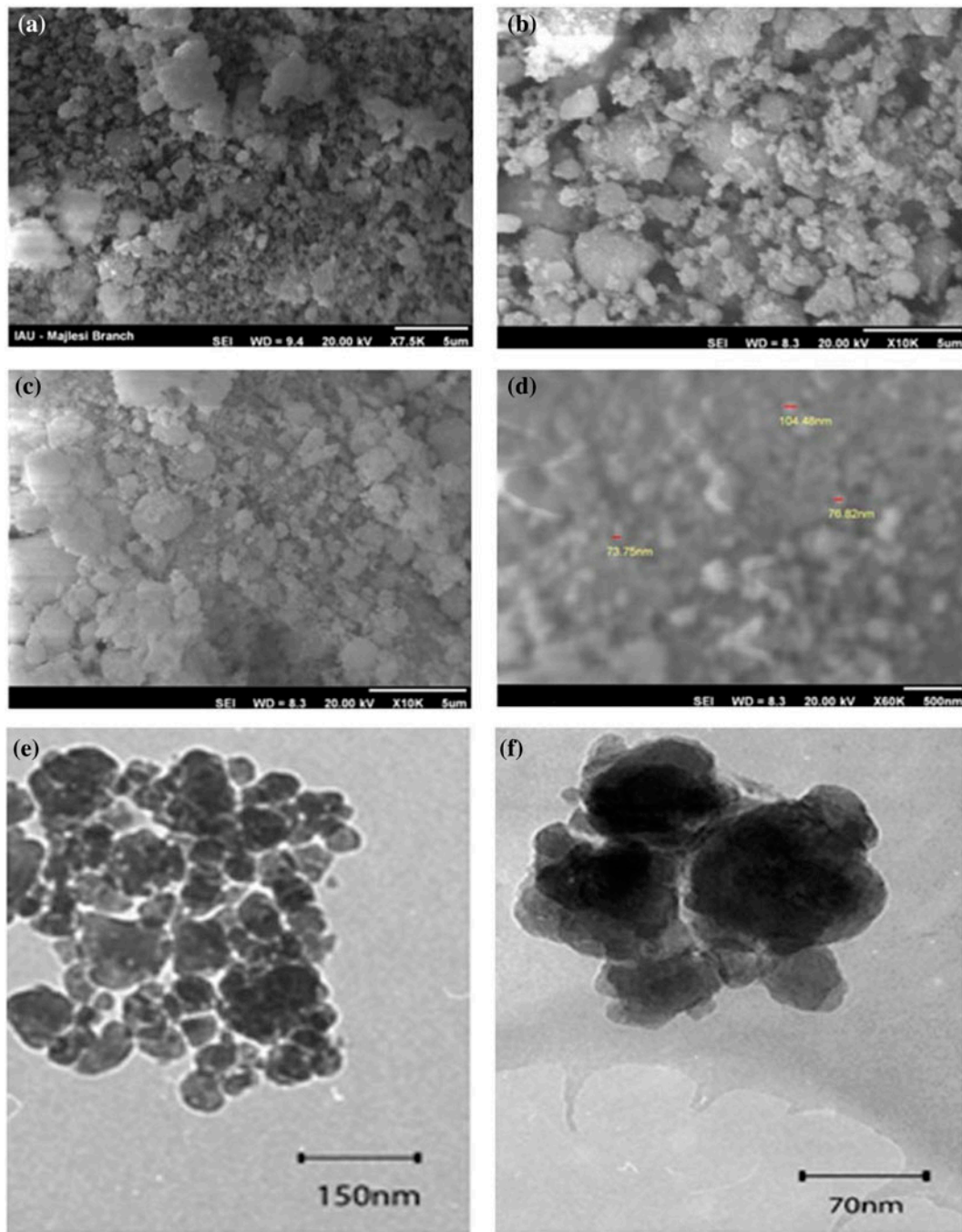
Fig. 3. SEM images of NCP (a), Fe–NCP (b), and FeO–NCP (c and d) and TEM images of NCP (e) and FeO–NCP (f).

the corresponding rate constants, k (min^{-1}), were calculated from the straight-line portion of the plots as a function of the semiconductor loading [27]. The k-values were, respectively, obtained as: 0.00003, 0.00015, 0.00017, and 0.0002 min^{-1} for FeO loadings of 1.6, 3.2, 3.7, and 4.1%. Based on the results, the catalyst containing 3.2% FeO (FeO$_{3.2\%}$–NCP; optimized catalyst) was used in later investigations.

3.2.2. Effect of initial phenol concentration

The influence of initial phenol concentration on the degradation process was investigated using 2, 5, and 10 times of diluted wastewater samples. Fig. 5 shows that the degradation percentage of five times-diluted wastewater sample increased and thereafter decreased. The produced hydroxyl radicals have a very short-life
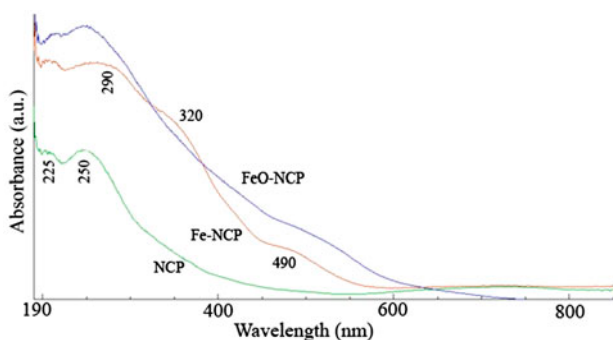
Fig. 4. DRS spectra of NCP, Fe–NCP, and FeO–NCP samples.

Table 2
The properties of the catalysts

Abbreviations of the catalysts	C_{Fe} (M)	FeO%
FeO 1.6%–NCP	0.05	1.6
FeO 3.2%–NCP	0.10	3.2
FeO 3.7%–NCP	0.20	3.7
FeO 4.1%–NCP	0.30	4.1

time about a few nanoseconds and should consume where they have formed. Hence, in many diluted samples (10 times), due to the presence of insufficient phenol molecules near the catalyst surface where hydroxyl radicals are formed, the degradation percent decreased. In this condition, hydroxyl radicals may react with together or attack other molecules in the environment. An increase in the concentration of phenol led to the decrease in number of photons that
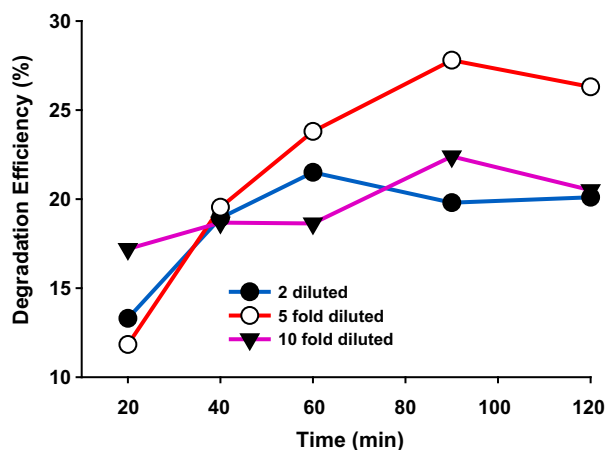

Fig. 5. Effect of FeO–NCP dosage on the degradation efficiency: initial phenol concentration of 100 mg L^{-1} (in five times-diluted wastewater); and initial pH 6.7.

arrived on the surface of the catalyst, hence, the produced hydroxyl radicals decreased [28,29]. As mentioned above, the best conditions to reach the best degradation percentage obtained using five times-diluted sample. The degradation of phenol was fitted in the following first-order kinetics equation:

$$\ln(C_0/C) = kt \tag{3}$$

where C_0 and C are the initial and final phenol concentrations at time t, respectively, and k, is the reaction rate constant. The rate constants, k (min^{-1}), were calculated from the slopes of the straight-line portion of the plotting of $\ln(C_0/C)$ vs. time [27] and the results are summarized in Table 3.

3.2.3. Effect of zeolite

After performing digestion on 0.1 g of FeO–NCP sample, its Fe content was determined by atomic absorption spectroscopy and the value was 7.3 mg (equal to 11.75 mg FeO) per gram of the sample. To

Table 3
Degradation rate constants (k) of phenol as a function of experimental parameters

Parameter	Value	$k \times 10^4$ (min^{-1})
C_{phenol} (Times of dilution)	2	1.0
	5	12.1
	10	8.7
Amount of catalyst (g L^{-1})[a]	0.1	1.6
	0.3	12.6
	0.5	4.5
	0.8	6.5
Solution pH[b]	3	3.3
	5.5	14.5
	6.7	13.3
	9	1.3
	11	7.1
C_{H2O2} (mmol L^{-1})[c]	50	72.3
	100	65.2
	200	110.1
C_{KBrO3} (mmol L^{-1})[d]	30	110.1
	50	150.0
	70	64.6

[a]Phenol concentration: five times diluted, and pH 6.7.
[b]Phenol concentration: five times diluted, amount of catalyst: 0.3 g L^{-1}.
[c]Phenol concentration: five times diluted, amount of catalyst: 0.3 g L^{-1}, and pH 6.7.
[d]Phenol concentration: five times diluted, pH 6.7, and amount of catalyst: 0.3 g L^{-1}.

study the role of nanoparticles of clinoptilolite on the degradation efficiency, some experiments were performed at the same conditions (initial solution pH 6.7; five times-diluted wastewater sample) using FeO as doped onto micronized and nanosized-clinoptilolite particles (FeO-MCP and FeO–NCP, respectively), bulk FeO, and raw NCP samples. The obtained results which are collected in Fig. 6 showed no considerable degradation activity for raw NCP and Fe–NCP samples. Although the bulk FeO had better activity with respect to NCP and Fe–NCP, the photocatalytic activity significantly increased by supported FeO onto both micronized and nanosized clinoptilolite particles, especially in case of nanoparticles because of higher effective surface area of nanoparticles. In the absence of zeolite, FeO particles tend to aggregate which decreased the active surface sites. But in the case of supported-FeO, regarding the small and definite pores size of the zeolite, small particles of FeO are present on the zeolite surface that increase the available active sites of the catalyst [30–32].

3.2.4. Effect of photocatalyst dose

The initial rate of the photocatalytic degradation of many pollutants is a function of the photocatalyst dosage [33]. A series of experiments were carried out by varying the amount of the catalyst from 0.1 to 0.8 g L^{-1} and the obtained results are depicted in Fig. 7. It is seen that the degradation efficiency was increased by increasing the mass of the catalyst from 0.1 to 0.3 g L^{-1}, and thereafter decreased. An increase in the photocatalyst dosage led to an increase in the
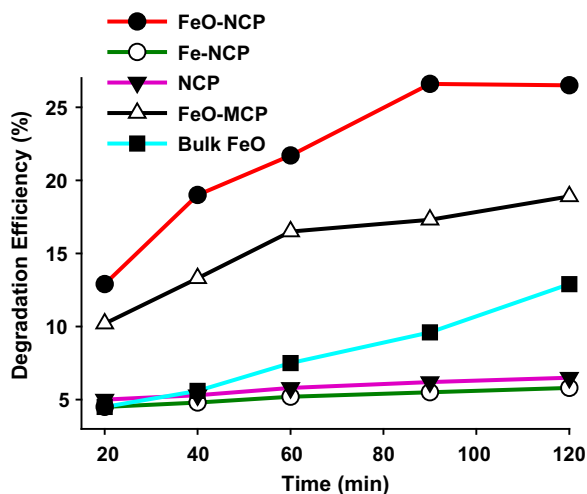
available active sites on the catalyst surface. In this case, the number of absorbed photons and also the number of adsorbed phenol molecules increased [34]. At catalyst mass beyond 0.3 g L^{-1}, the penetration of photons decreased by the aggregated solid particles. On the other hand, an increase in the turbidity of suspension led to reduction in the light transmission through the suspension which in turn decreased the overall number of photons that reached the catalyst particles and the production of OH radicals [35,36]. The corresponding rate constants, k (min^{-1}), are listed in Table 3.

3.2.5. Effect of pH

The pH of an aquatic environment plays an important role on the photocatalytic degradation of organic substances since determines the surface charge of the photocatalyst and the size of formed aggregates [37,38]. The effect of pH (3–11) on the photodegradation extent of phenol in the proposed wastewater was investigated in a series of five times-diluted wastewater suspensions containing 0.3 g L^{-1} of the catalyst. The obtained results which are presented in Fig. 8 show the highest degradation efficiency at pH 6.7. At the strong acidic pHs, due to acidification of the suspension by HCl, a high amount of chloride anions is added to the solution. These can react with hydroxyl radicals leading to formation of the $CLO^{-\cdot}$ radical ions. The produced new radicals are much lower reactive than hydroxyl radicals. At the strong acidic pHs, the partially repulsive forces between the positively protonated catalyst surface (due to surface adsorption of protons) and partially protonated phenol molecules
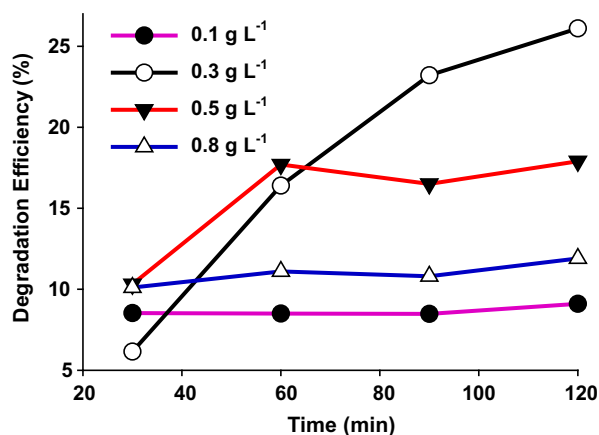
Fig. 6. Effect of zeolite on FeO photocatalytic activity: 0.3 g L^{-1} catalysts; initial phenol concentration of 100 g L^{-1} (in five times-diluted wastewater); and initial pH 6.7.

Fig. 7. Effect of solution pH on the degradation efficiency of phenol: 0.3 g L^{-1} catalyst; and initial phenol concentration of 100 mg L^{-1} (in five times-diluted wastewater).
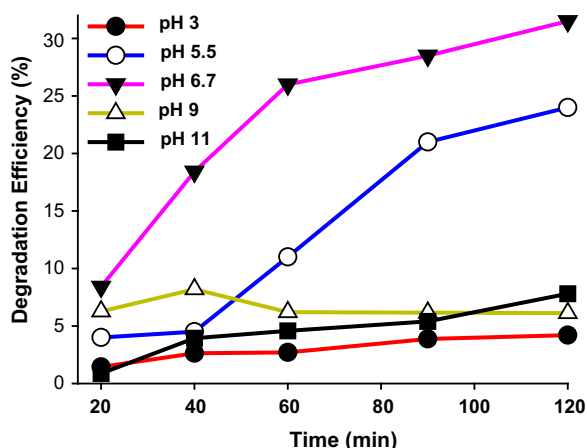
Fig. 8. Effect of initial concentration of phenol on the degradation efficiency: 0.3 g L^{-1} catalyst; and initial pH 6.7.

can also away the phenol molecules from the surface of the catalyst, where the hydroxyl radicals produced. In addition, acidic conditions may also dissolve FeO from the catalyst surface. The leached iron in the solution at the end of photodegradation process was checked qualitatively by atomic absorption spectroscopy. Due to low extent of leached iron no iron was detected at pHs > 3 and only little leached irons were detected qualitatively at pH 3. This confirms that the degradation process was done via a heterogeneous process. These are major reasons for reducing the photodegradation extent of phenol at the strong acidic pHs which are in agreement with literature [39]. As shown, the degradation efficiency decreased also at strong basic pHs due to probably repulsive forces between the negative charges of the catalyst surface, because of adsorption of sufficient hydroxyl anions, and free electrons of oxygen atoms of phenol molecules. In addition, acidic conditions may also dissolve FeO from the catalyst surface. This phenomenon was checked qualitatively by atomic absorption spectroscopy due to the low extent of leached iron and the results confirmed that more leached irons at the strongest acidic pHs. Hence, the degradation percent of phenol was decreased at strong acidic conditions [39]. This also confirms that the degradation process was done via a heterogeneous process. As shown, the degradation efficiency decreased also at strong basic pHs due to the probably repulsive forces between the negative charges of the catalyst surface because of the adsorption of sufficient hydroxyl anions and the free electrons of oxygen atoms of phenol molecules. The point of zero charge (pH$_{pzc}$) of FeO has been reported at pH 8.6–9.3 [40]. It is possible that by supporting

FeO onto the clinoptilolite, these values change to 6.7. As we know, above this point, the surface of FeO–NCP has a net negative charge while below pH$_{pzc}$, it has a net positive charge. Hence, at pH 6.7, the mentioned repulsive forces diminished which led to an increase in the degradation of phenol molecules. These observations are coherent with the literature that confirmed the phenol degradation to be favorable in the mild acidic and neutral solutions [41]. The rate constant values, k (min^{-1}), as a function of the solution pH are also summarized in Table 3.

3.2.6. Effect of electron acceptors

The initial concentration of H$_2$O$_2$ plays an important role in the degradation extent of organic pollutants. Oxidizing agents like H$_2$O$_2$, Na$_2$BO$_3$, K$_2$S$_2$O$_8$, KBrO$_3$, KIO$_3$, and KIO$_4$ enhance the efficiency of photodegradation processes. The addition of external oxidant/electron acceptors into a semiconductor suspension has led to improve the photocatalytic degradation of organic contaminants by: (a) preventing the electron–hole recombination by accepting the conduction band electrons; (b) increasing the hydroxyl radicals concentration; and (c) generating more radicals and other oxidizing species to accelerate the degradation of intermediate compounds [41]. Fig. 9 displays the effect of hydrogen peroxide dosage on the degradation extent of phenol molecules. As shown, an increase in the H$_2$O$_2$ concentration from 50 mmol L^{-1} to 200 mmol L^{-1} led to an increase in the degradation extent of phenol molecules. On the other hand, H$_2$O$_2$ increases the concentration of hydroxyl radicals according to the following reactions [41,42]:
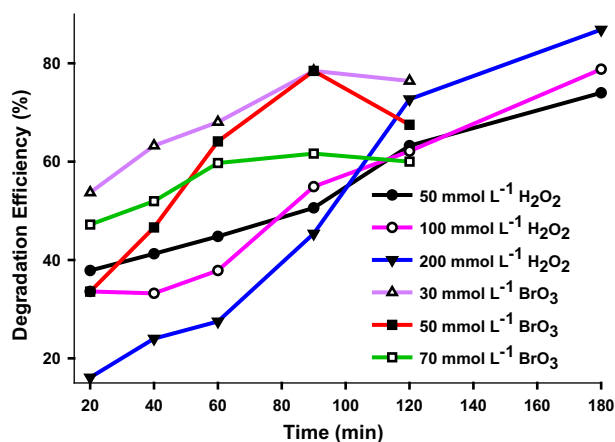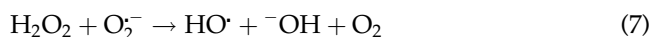

Fig. 9. Effect of the hydrogen peroxide and potassium bromate concentration on degradation efficiency of phenol: 0.3 g L^{-1} catalyst; initial solution pH 6.7; and initial phenol concentration of 100 mg L^{-1}.

$$H_2O_2 + e^- \rightarrow {}\cdot OH + OH^- \qquad (4)$$

$$H_2O_2 \rightarrow {}\cdot OH + OH^- \qquad (5)$$

The added H_2O_2 can also scavenge electrons from the conduction band of FeO–NCP to generate excess hydroxyl radicals (reactions 3 and 4). H_2O_2 molecules can also generate hydroxyl radicals by direct hemolytic fission in the presence of UV light based on the reaction (6):

$$H_2O_2 + (FeO-NCP)e^- \rightarrow HO^{\cdot} + {}^-OH \qquad (6)$$

$$H_2O_2 + O_2^{\cdot-} \rightarrow HO^{\cdot} + {}^-OH + O_2 \qquad (7)$$

$$H_2O_2 + h\nu \rightarrow 2HO^{\cdot} \qquad (8)$$

The effect of added bromate anions on the degradation extent of phenol was also studied and the results are shown in Fig. 9. As shown, a 50-mmol L^{-1} bromate showed better degradation rate due to the reaction between BrO_3^- and conduction band electrons. This reduces the recombination of electron–hole pairs.

$$BrO_3^- + 6e^- + 6H^+ \rightarrow Br^- + 3H_2O \qquad (9)$$
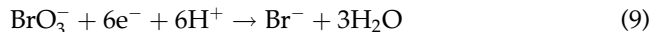
Higher doses of bromate anions have a negative effect due to the reaction of bromate ions with hydroxyl radicals. Based on the results, lower doses of bromate with respect to hydrogen peroxide led to higher enhancement of the degradation of phenol.

3.2.7. Reusing of the catalyst

The reusing tests were performed in order to evaluate the catalytic activity of FeO–NCP catalyst during successive using. For this goal, the used catalysts were regenerated at two drying temperatures of 100 and 200°C. The reused catalyst was used in five successive experiments and at the beginning of each

Table 4
Results of reusing of the catalyst

Degradation% at dried temperatures of:	
200°C	100°C
32.4	26.4
30.0	23.2
23.5	18.0
17.0	12.0

run, the phenol concentration and catalyst amount were adjusted back to the initial values (10 mL of five times-diluted wastewater, pH 6.7, and 0.3 g L^{-1} catalyst). At the end of the photodegradation process, the catalyst was removed, washed with water for several times, and dried. It is obvious that the initial activity was decreased gradually during the successive runs (Table 4). The decay of active catalytic sites is considered as the reason for this initial loss of activity [43]. Also, the deposition of photodegradation products on catalyst surface can block and cover the surface, and decrease the degradation activity of the reused catalysts. Hence, an increase in the drying temperature from 100 to 200°C led to remove the intermediates from the catalyst surface. This causes an increase in the activity of the reused catalysts [44,45].

3.2.8. Confirmation of the degradation of phenol

Fig. 10 shows a decrease in the absorbance of the wastewater sample during 60 min irradiation time. As shown, the absorbance of the sample decreased with the progress of the photodegradation process which confirms a decrease in the concentration of phenol due to its destruction. HPLC was also used for confirming the degradation of phenol in the proposed wastewater sample. The corresponding HPLC chromatograms of the used sample during a 120 min photodegradation process are shown as inset of Fig. 10. As shown, a sharp decrease in the peak intensity was observed due to the degradation of phenol. COD was another technique for confirming the photodegradation results. The remained COD values of 2,050, 1,670,
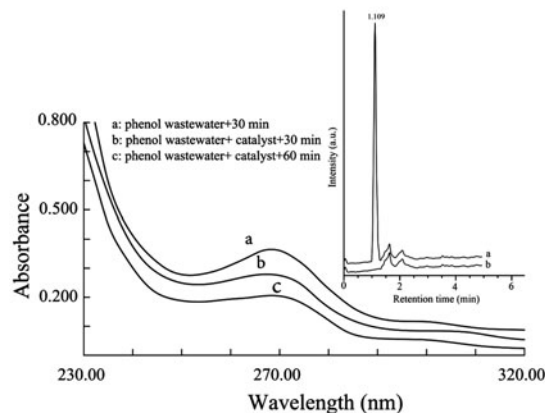
Fig. 10. Decrease in UV–vis absorption spectra of phenol in the proposed wastewater sample during the photodegradation process (inset: HPLC chromatogram of the proposed phenolic wastewater a: before and b: after 120 min photodegradation process).

1,450, 1,330, and 1,210 mg L^{-1} are obtained during photodegradation times of 0, 40, 60, 100, and 120 min, respectively. However, the HPLC and COD results are in agreement with the UV–vis results confirming the degradation of phenol in the proposed wastewater to smaller fragments.

To confirm the complete degradation of pollutants present in the wastewater sample, photodegradation of a sample was studied under the optimized conditions and the reduction of TOC was followed. The initial TOC of 3,500 mg L^{-1} of the subjected sample decreased to 2,730, 2,415, 2,135, and 1,610 mg L^{-1} at irradiation times of 40, 60, 90, and 120 min, respectively. These values correspond to the degradation extents of 22, 31, 39, and 54% which are greater than the values obtained by spectrophotometric measurements. On the other hand, in spectrophotometric measurements because of the measurement of absorbance of samples at a maximum absorption wavelength of phenol, only the degraded phenol molecules are measured. But, TOC results confirm that in addition of the degradation of phenol molecules, other organic molecules present in the wastewater sample can be also degraded by the proposed catalyst. Hence, the proposed catalyst can be used for effective removal of the pollutants present in the proposed wastewater sample.

4. Conclusion

The results of this work confirm that the supporting of FeO onto a zeolitic bed improves its photocatalytic reactivity because zeolite can prevent from the aggregation of FeO particles and also recombination of the electron–hole pairs. Also, usage of nanoparticles of zeolite significantly increased the activity of the obtained composite with respect to the micronized one. About 25–30% of phenol molecules degraded in the used wastewater sample without electron acceptors which is significant for a real wastewater sample with respect to the common synthetic solution samples. Hence, the results confirm the effectiveness of the proposed FeO–NCP catalyst for the degradation of a phenol-contained wastewater. The presence of hydrogen peroxide and potassium bromate significantly increased the photodegradation extent because of their important role to prevent the electron–hole recombination.

References

[1] V.G. Gandhi, M.K. Mishra, P.A. Joshi, A study on deactivation and regeneration of titanium dioxide during photocatalytic degradation of phthalic acid, J. Ind. Eng. Chem. 18 (2012) 1902–1907.

[2] Y.-J. Jung, Y. Kiso, K.-H. Kwon, Y. Kamimoto, K.-S. Min, Biological removal characteristics of phenol with filtration bio-reactor, Desalin. Water Treat. 53 (2015) 3096–3103.

[3] L. Zhang, J. Liu, C. Tang, J. Lv, H. Zhong, Y. J. Zhao and X. Wang, Palygerskite and SnO_2–TiO_2 for the photodegradation of phenol, Appl. Clay Sci. 51 (2011) 68–73.

[4] Ch.-H. Chiou, Ch.-Y. Wu, R.-Sh. Juang, Photocatalytic degradation of phenol and *m*-nitrophenol using irradiated TiO_2 in aqueous solutions, Sep. Purif. Technol. 62 (2008) 559–564.

[5] J.K. Yang, S.M. Lee, M. Farrokhi, O. Giahi, M. Shirzad Siboni, Siboni, Photocatalytic removal of Cr(VI) with illuminated TiO_2, Desalin. Water Treat. 46 (2012) 375–380.

[6] A. Nezamzadeh-Ejhieh, N. Moazzeni, Sunlight photodecolorization of a mixture of Methyl Orange and Bromocresol Green by CuS incorporated in a clinoptilolite zeolite as a heterogeneous catalyst, J. Ind. Eng. Chem. 19 (2013) 1433–1442.

[7] M.R. Samarghandi, J.K. Yang, S.M. Lee, O. Giahi, M. Shirzad-Siboni, Effect of different type of organic compounds on the photocatalytic reduction of Cr(VI) in presence of ZnO nanoparticles, Desalin. Water Treat. 52 (2014) 1531–1538.

[8] A. Nezamzadeh-Ejhieh, M. Karimi-Shamsabadi, Comparison of photocatalytic efficiency of supported CuO onto micro and nano particles of zeolite X in photodecolorization of Methylene blue and Methyl orange aqueous mixture, Appl. Catal. A: Gen. 477 (2014) 83–92.

[9] A. Nezamzadeh-Ejhieh, F. Khodabakhshi-Chermahini, Incorporated ZnO onto nano clinoptilolite particles as the active centers in the photodegradation of phenylhydrazine, J. Ind. Eng. Chem. 20 (2014) 695–704.

[10] N.M. Mahmoodi, Magnetic ferrite nanoparticle–alginate composite: Synthesis, characterization and binary system dye removal, J. Taiwan Inst. Chem. Eng. 44 (2013) 322–330.

[11] A. Nezamzadeh-Ejhieh, Z. Banan, Sunlight assisted photodecolorization of crystal violet catalyzed by CdS nanoparticles embedded on zeolite A, Desalination 284 (2012) 157–166.

[12] F.B. Li, X.Z. Li, X.M. Li, T.X. Liu, J. Dong, Heterogeneous photodegradation of bisphenol A with iron oxides and oxalate in aqueous solution, J. Colloid Interface Sci. 311 (2007) 481–490.

[13] C. Wang, H. Shi, Y. Li, Synthesis and characteristics of natural zeolite supported Fe^{3+}–TiO_2 photocatalysts, Appl. Surf. Sci. 257 (2011) 6873–6877.

[14] L. Song, R. Qiu, Y. Mo, D. Zhang, H. Wei, Y. Xiong, Photodegradation of phenol in a polymer-modified TiO_2 semiconductor particulate system under the irradiation of visible light, Catal. Commun. 8 (2007) 429–433.

[15] M.S. Nahar, K. Hasegawa, S. Kagaya, S. Kuroda, Adsorption and aggregation of Fe(III)–hydroxy complexes during the photodegradation of phenol using the iron-added–TiO_2 combined system, J. Hazard. Mater. 162 (2009) 351–355.

[16] E.M. Flanigen, H. Khatami, H.A. Szymanski, Molecular Sieve Zeolite I, Academic Press, New York, NY, 1971, p. 201.

[17] M. Brazlauskas, S. Kitrys, Synthesis and properties of CuO/Zeolite sandwich type adsorbent-catalysts, Chin. J. Catal. 29 (2008) 25–30.

[18] M.K. Doula, Synthesis of a clinoptilolite-Fe system with high Cu sorption capacity, Chemosphere 67 (2007) 731–740.

[19] A. Filippidis, A. Godelitsas, D. Charistos, P. Misaelides, A. Kassoli-Fournaraki, The chemical behavior of natural zeolites in aqueous environments: Interactions between low-silica zeolites and 1 M NaCl solutions of different initial pH-values, Appl. Clay Sci. 11 (1996) 199–209.

[20] R. Silverstein, G.C. Bassler, T.C. Morill, Spectromatic Identification of Organic Compounds, Wiley, New York, NY, 1981.

[21] M. Doula, A. Ioannou, A. Dimirkou, Copper adsorption and Si, Al, Ca, Mg, and Na release from clinoptilolite, J. Colloid Interface Sci. 245 (2002) 237–250.

[22] M.A. Kcay, FT-IR spectroscopic investigation of the adsorption pyridine on the raw sepiolite and Fe-pillared sepiolite from Anatolia, J. Mol. Struct. 694 (2004) 21–26.

[23] M. Akgül, A. Karabakan, Promoted dye adsorption performance over desilicated natural zeolite, Microporous Mesoporous Mater. 145 (2011) 157–164.

[24] A. Chen, M. Xiaodong, S. Hongwen, Decolorization of KN-R catalyzed by Fe-containing Y and ZSM-5 zeolites, J. Hazard. Mater. 156 (2008) 568–575.

[25] B. Concepción-Rosabal, J. Balmaceda-Era, G. Rodríguez-Fuentes, Characterization of Fe^{2+}-containing natural clinoptilolite and its interaction with saccharides, Microporous Mesoporous Mater. 38 (2000) 161–166.

[26] S. Davoodi, F. Marahel, M. Ghaedi, M. Roosta, A. Hekmati Jah, Tin oxide nanoparticles loaded on activated carbon as adsorbent for removal of Murexide, Desalin. Water Treat. 52 (2014) 7282–7292.

[27] A. Nezamzadeh-Ejhieh, Z. Banan, Kinetic investigation of photocatalytic degradation of dimethyldisulfide by zeolite A containing nano CdS, Iran. J. Catal. 2 (2) (2012) 77–81.

[28] A. Nezamzadeh-Ejhieh, S. Hushmandrad, Solar photodecolorization of methylene blue by CuO/X zeolite as a heterogeneous catalyst, Appl. Catal. A: Gen. 388 (2010) 149–159.

[29] Q. Zhang, W. Jiang, H. Wang, M. Chen, Oxidative degradation of dinitro butyl phenol (DNBP) utilizing hydrogen peroxide and solar light over a Al_2O_3- supported Fe(111)-5-sulfososalicylic acid (ssal) catalyst, J. Hazard. Mater. 176 (2010) 1058–1064.

[30] Z.M. El-Bahy, M.M. Mohamed, F.I. Zidan, M.S. Thabet, Photo-degradation of acid green dye over Co–ZSM-5 catalysts prepared by incipient wetness impregnation technique, J. Hazard. Mater. 153 (2008) 364–371.

[31] M. Alvaro, E. Carbonell, M. Esplá, H. Garcia, Iron phthalocyanine supported on silica or encapsulated inside zeolite Y as solid photocatalysts for the degradation of phenols and sulfur heterocycles, Appl. Catal. B: Environ. 57 (2005) 37–42.

[32] A. Nezamzadeh-Ejhieh, Z. Salimi, Heterogeneous photodegradation catalysis of o-phenylenediamine using CuO/X zeolite, Appl. Catal. A: Gen. 390 (2010) 110–118.

[33] A. Nezamzadeh-Ejhieh, S. Khorsandi, Photocatalytic degradation of 4-nitrophenol with ZnO supported nano-clinoptilolite zeolite, J. Ind. Eng. Chem. 20 (2014) 937–946.

[34] Y. Jiang, Y. Sun, H. Liu, F. Zhu, H. Yin, Solar photocatalytic decolorization of C. I. Basic Blue 41 in an aqueous suspension of TiO_2-ZnO, Dyes Pigm. 78 (2008) 77–83.

[35] M.B. Kasiri, H. Aleboyeh, A. Aleboyeh, Decolorization of acid blue 74 using Fe-ZSM5 zeolite as a heterogeneous photo-fenton catalyst, Appl. Catal. B: Environ. 84 (2008) 9–15.

[36] M. Pera-Titus, V. García-Molina, M.A. Baños, J. Giménez, S. Esplugas, Degradation of chlorophenols by means of advanced oxidation processes: A general review, Appl. Catal. B: Environ. 47 (2004) 219–256.

[37] H.K. Singh, M. Saquib, M. Haque, M. Muneer, Titanium dioxide mediated photocatalysed degradation of phenoxyacetic acid and 2,4,5-trichlorophenoxyacetic acid, in aqueous suspensions, J. Mol. Catal. A: Chem. 264 (2007) 66–72.

[38] A. Nezamzadeh-Ejhieh, M. Bahrami, Investigation of the photocatalytic activity of supported ZnO–TiO_2 on clinoptilolite nano-particles towards photodegradation of wastewater-contained phenol, Desalin. Water Treat. (2014), doi:10.1080/19443994.2014.922443.

[39] C. Karunakaran, R. Dhanalakshmi, P. Gomathisankar, G. Manikandan, Enhanced phenol-photodegradation by particulate semiconductor mixtures: Interparticle electron-jump, J. Hazard. Mater. 176 (2010) 799–806.

[40] S. Ahmed, M.G. Rasul, W.N. Martens, R. Brown, M.A. Hashib, Heterogeneous photocatalytic degradation of phenols in wastewater: A review on current status and developments, Desalination 261 (2010) 3–18.

[41] J.R. Rustad, E. Wasserman, A.R. Felmy, Molecular modeling of the surface charging of hematite, Surf. Sci. 424 (1999) 28–35.

[42] I. Peternel, N. Koprivanac, H. Kusic, UV-based processes for reactive azo dye mineralization, Water Res. 40 (2006) 525–532.

[43] M. Tekbaş, H.C. Yatmaz, N. Bektaş, Heterogeneous photo-Fenton oxidation of reactive azo dye solutions using iron exchanged zeolite as a catalyst, Microporous Mesoporous Mater. 115 (2008) 594–602.

[44] K. Venkata Subba Rao, M. Subrahmanyam, P. Boule, Immobilized TiO_2 photocatalyst during long-term use decrease of its activity, Appl. Catal. B: Environ. 49 (2004) 239–249.

[45] M. Huang, Ch Xu, Z. Wu, Y. Huang, J. Lin, J. Wu, Photocatalytic discolorization of methyl orange solution by Pt modified TiO_2 loaded on natural zeolite, Dyes Pigm. 77 (2008) 327–334.